Title
10-MeV PROTON REACTION CROSS SECTION FOR SEVERAL ELEMENTS

Authors
Wilkins, Bruce D.
Igo, George.

Publication Date
1962-08-06

UCRL-10281

University of California

Ernest O. Lawrence Radiation Laboratory

Berkeley, California

DISCLAIMER

Submitted for Pub. in Physical Review

UCRL-10281

UNIVERSITY OF CALIFORNIA

Lawrence Radiation Laboratory
Berkeley, California

Contract No. W-7405-eng-48

10-MeV PROTON REACTION CROSS SECTIONS FOR SEVERAL ELEMENTS

Bruce D. Wilkins and George Igo

August 6, 1962

10- MeV PROTON REACTION CROSS SECTIONS FOR SEVERAL ELEMENTS

Bruce D. Wilkins and George Igo

Lawrence Radiation Laboratory
University of California
Berkeley, California

August 6, 1962

ABSTRACT

We have obtained proton nonelastic cross sections at 10 MeV from Be, C, Al, Ti, Mo, Zr, Fe, Ni, Zn, Cu, V, Rh, Nb, Ag, Sn, Ta, Th, Au, and Pb. The most significant feature of the data is the appearance of two strong minima in the elements lighter than Cu. The data are compared with optical-model predictions. These calculations predict the right order for the reaction cross section when a surface absorption potential that fits existing elastic-scattering data is used. However, on the basis of our data, a volume absorption potential of the Woods-Saxon shape cannot be excluded. The data are compared with other measurements of nonelastic cross sections for 10-MeV protons.

10-MeV PROTON REACTION CROSS SECTIONS FOR SEVERAL ELEMENTS

Bruce D. Wilkins and George Igo

Lawrence Radiation Laboratory
University of California
Berkeley, California

August 6, 1962

I. INTRODUCTION

Until recently, reaction cross sections were not available to test optical-model predictions for protons. The first measurements by Gooding[1] at Minnesota were made at 34 MeV. Later work at Minnesota that used the same equipment at 61 MeV has also been reported.[2] These results were used to test the results of the extensive optical-model analysis of elastic-scattering proton data by Glassgold and his collaborators[3] in 1958. This analysis has shown that a volume-absorption potential of the same spatial dimension as the real potential (the Woods-Saxon potential)[4] was adequate to fit the elastic-scattering data, and that furthermore, there was ambiguity particularly in the depth of the potential V and the size of the nuclear radius R. The quantity VR^2 needed only to be fixed within a fairly wide range in V and R, the so called VR^2 ambiguity. The Minnesota reaction cross-section results served to put some rather broad limits on the range which the optical-model parameters could take on; however, better accuracy was needed to seriously restrict the parameters of the optical model. Certainly there was no indication from these results that the Woods-Saxon potential would not serve.[4] The analysis showed in fact, that 1 or 2% accuracy in the reaction cross section was necessary to put restrictions on the optical-model parameters. The work reported in this paper is an effort in this direction. The error introduced due to counting statistics in the results that will be quoted below are of the order of 2% and can be obtained in a reasonable length of time (about 20 minutes). Higher statistical accuracy

could of course be obtained in a suitable longer period of time.

It has been pointed out by Hintz[5] and Greenlees[6] that proton reaction cross sections measured at energies near the coulomb barrier should be especially sensitive to the nuclear potentials, since small variations in barrier height due to the shape and character of the nuclear potential can alter reaction cross sections by a large amount. A series of experiments or summaries of relevant data to test this suggestion in the vicinity of 10 MeV have been reported.[7-12] This work is summarized in the next paragraph.

Meyer and Hintz[7] collected all the data available at that time on partial cross sections induced by protons at 9.85 MeV, particularly the (p, n) and (p, q. . .) cross section, where q is any charged particle. Their cross sections do not include values for the (p, γ) reaction but this is expected to be small (1 to 2 mb).[7, 8] Later Albert and Hansen[9] published new measurements of σ(p, n) at 9.85 MeV that they combined with the Meyer and Hintz[7] charged-particle cross section and with (p, 2n) contributions that were estimated, --using the statistical model of the nucleus.[14] Recently Wing and Huizenga[10] measured the (p, n) cross section in this energy region. Benveniste[11] has also measured σ(p, q) for Cu. Two experiments have been performed at about 10 MeV to measure the reaction cross section for Cu by direct attenuation of the beam. Greenlees[8] has used a method involving the measurement of the unattenuated beam I_0 and the attenuated beam I by rotating a Au sample and a Cu sample of the same stopping power into the beam alternately and measuring the variation in count rate in a stopping counter. The power of the method rests on the rapid alternation of the measurement of I_0 (Au target in) and I (Cu target in), thus averaging out variations in beam intensity. The Au target attenuation is small so that only a small correction need be made. Of course, in addition a correction for elastic scattering of beam protons outside of the angular interval subtended by the back counter must be made for Au. However, since this is

almost pure coulomb scattering, the correction factor, although larger than that due to the attenuation in the Cu target, is well-known. In order to reduce the error to a reasonable value, 100 hours of machine time were required. As will be discussed below, the method reported in this paper requires 20 minutes to obtain 2% statistical uncertainty in the reaction cross section for each target. Carlson et al.,[12] using a method involving the measurement of I_0-I, also obtained a value for Cu. The method is very similar to ours but utilizes slower electronic equipment, and consequently required more than a week of running time on a low-duty-cycle machine to reduce the error to 8%. Recent measurements by these two groups yield values of 930±70 mb[8] at 9.3 MeV and 970±75 mb[12] at 9 MeV. Pollock and Schrank, using a technique similar to ours, have reported results for 16.6-MeV protons.[13]

The results of Greenlees and Jarvis,[8] Carlson et al.[12] tend to be larger than the results of the experiments in which σ_R is found by summing the pertinent partial cross sections.[7, 9, 10] The measurements reported in this paper are in accord with the latter experimental results. The present measurements at 10 MeV lead to the following conclusions about the applicability of the optical model with various form factors. An optical model that uses a volume-absorption potential of the same shape and radius as the real potential (i.e. the Woods-Saxon potential) predicts a range of reaction cross sections, the upper limit of which nears the experimental values.[4] A surface-absorption potential that reaches a maximum at the half-value radius of the real potential can be adjusted to fit the elastic-scattering data and also fit the trend of the reaction cross-section measurements.[15, 16] It has also been pointed out by Hodgson that the data can be fitted equally well by volume-absorption potentials if we relax the requirement that the radii of the real and imaginary parts of the potential should be equal.[17]

II. EXPERIMENTAL METHOD

Previous measurements using the attenuation method[1, 8, 12] had involved considerable amounts of accelerator time. Consequently the statistical accuracy and number of elements measured were always small. Another method based on summing partial reaction cross sections is practical only at low bombarding energies. It has been applied in a few cases in which all of the reactions with appreciable cross sections have been measured.[7, 9, 10]

We shall discuss a method that requires about 20 minutes to obtain the raw data for a measurement with ~ 2% statistical accuracy using a CW, 60-inch-cyclotron beam. The 60-inch cyclotron produces a well-focused beam of 24-MeV H_2^+ ions outside the cyclotron shielding. Utilizing the cyclotron beam for these measurements required several criteria to be met. First of all, the beam intensity I_0 used in the experiment is very small, of the order of 5×10^4-sec^{-1} protons. Several serious experimental problems arise when such a configuration is used with the 60-inch cyclotron. First of all, it is hard to keep the beam constant at times, since the ion source must be run low and tends to be unstable. If the beam jumps up by several orders of magnitude, as it may do, it is quite possible to damage the plastic scintillators in the counting apparatus. Also the beam tends to be bunched at low power levels, owing to the 360-cycle ripple in the radio-frequency power level. This effect can reduce the time when the beam is on by a very large factor at low power levels and increase the data-collecting time. Furthermore, it is not possible to use this arrangement at all in the case of molecular hydrogen, where it is first necessary to disrupt the molecular bonds and produce hydrogen atoms.

There are, of course, several ways to meet the difficulties presented above. We have decided to produce a beam of ions for this measurement by

elastic scattering of a small portion of the available external beam. The beam preparation is shown schematically in Fig. 1, and the parameters for the proton measurements are quoted below. The external beam for the 60-inch cyclotron is focused by a quadrupole and a bending magnet on a 1/8 in. diameter tantalum collimator slightly thicker than the range of the ion in the beam and followed by an antiscattering baffle. Considerable care was taken to reduce the residual gas pressure in the system. When this was done, it was found possible to focus a 1-μA beam through the collimator. This beam was incident on a scattering foil that for some measurements was a lead foil enriched in Pb^{208} ($\Delta E \approx 1.0$ MeV for 12-MeV H^+ ions) and a thorium foil of approximately the same stopping power for the rest of the measurements (see Table II). A heavy-element scattering foil was chosen because the cross section at small angles is mainly coulomb elastic scattering, and therefore the number of undesirable low-energy protons produced by (p,p') reactions is reduced. In addition, the large cross section for coulomb scattering from heavy elements reduces the intensity requirement on the cyclotron beam. The isotope Pb^{208} was chosen because the first excited state in Pb^{208} is at an energy of 2.6 MeV, and therefore inelastic protons would be at least 2.6 MeV lower in energy than elastically scattered protons from reactions with Pb^{208}. Unfortunately other lead isotopes were present in relatively small percentages, and (p, p') reactions with these isotopes put a limit on the energy resolution obtainable in this experiment.

Scattered particles at 15° can pass through a collimating system consisting of two anti-wall scattering baffles and then through a 0.062-in. - collimator, placed 10 in. from the lead foil, followed by an antiscattering baffle. The baffles and the collimator are constructed of tantalum of a thickness just sufficient to stop protons, to reduce slit-scattering effects to a minimum. The collimated beam produced by this system passes through two 3-mil-thick plastic scintillators (counter 1 and counter 3) spaced 22 in. apart. Counter 1 is subject to a

heavy electron bombardment from the lead foil in the absence of a magnetic clearing field. A magnet placed close to the lead foil prevented the electrons (maximum energy ~20 KeV) from reaching counter 1. This is important since it sets the upper limit on the counting rate. This is so because at too high counting rates in counter 1 the pulse-height response becomes unsteady owing to high-current phenomena in the phototube.

In order to remove protons multiply-scattered away from the axis of the beam line, a 0.180-in.-plastic scintillator collimator counter (counter 2) was placed directly in front of counter 3. Counter 1 and counter 3 output pulses were put into fast coincidence ($\tau \approx 2$ mμsec), and pulses from counter 2, after having passes through a tunnel diode discriminator circuit[18] that produces shaped pulses of uniform height and of width 20 mμsec, were put into anticoincidence. By utilizing the time-of-flight separation resulting from the 22-in. flight path S, (p, p') events from Pb^{208} can be reasonably well separated, since the first excited state yields 7.2-MeV protons. The time-of-flight requirement is capable of separating out anything less than 7.4 MeV with good efficiency since $\delta E/E \approx \frac{2\tau}{S}\sqrt{\frac{2E}{m}} \approx 0.33$, where E = 11 MeV, and m is the proton mass. Some (p, p') events from other isotopes of lead in the enriched Pb^{208} scattering foil cannot be removed, since the first excited states are closer to the ground state. In the case of the thorium scatterer, the (p, p') cross section is almost negligible, since the coulomb barrier is high. In addition, slit-scattered particles not removed by the collimation system may contribute particles that are not removed by the time-of-flight technique. Great care was taken to insure that there were no sources of scattering after counter 1. As an example of this, counter 2 was made an anticoincidence collimator counter in place of an ordinary metal collimator; and all beam-tube dimensions were made large enough to remove the possibility of wall scattering. Multiple coulomb scattering of the protons in counter 1 removed 85% of

the protons from the beam, i.e. only 15% of the protons passing through counter 1 also pass through the 0.180-in. hole in counter 2. This means that the counting rate in counter 1 is about seven times as high as in any of the other counters. Therefore it limited the counting rate in the experiment because, as mentioned above, if the counting rate is too high then the pulse height becomes unstable. The counter-1 counting rate was about 5×10^5 sec^{-1}. The coincidence rate for the kind of event 1 $\overline{2}$ 3 (where by the upper bar we mean that counter 2 is in anticoincidence) is, however, very close to the maximum rate allowable from another consideration. We obtain an event 1 $\overline{2}$ 3 in every 240 rf bursts. If we obtained one in every 100 rf bursts with a perfectly uniform beam, we could expect that in 1% of the time two protons would pass through the apparatus in 1 rf burst and introduce a 1% correction to the experimental result. Since in fact the beam does show some structure associated with the rf voltage (f = 360 sec^{-1}) even under the best operating conditions, one would probably settle for a value of I_0 of the order of magnitude that it has.

All counters following counter 2 are mechanically aligned with respect to counter 2. However, the 22-in. pipe connecting counter 1 and counter 2 is relatively flexible so that the assembly may be aligned with respect to the beam line defined by the beam spot on the scattering foil and on the 0.062-in. collimator preceding counter 1. This is easily accomplished by recording the number of 1 $\overline{2}$ 3 events vs integrated incident beam as measured in the Faraday cup (see Fig. 1). When the apparatus is slightly out of line so that a large proportion of the protons is striking counter 2, the 1 $\overline{2}$ 3 counting rate is greatly reduced. This effect allows accurate alignment.

The monitor counter at 60° (see Fig. 1) receives some scattered radiation. The photomultiplier output is displayed on an oscilloscope triggered by the

60-cycle main power so that the operator can view the gross beam structure introduced by the 360-cycle modulation on the rf voltage discussed above. The operator can then readily optimize machine paramenters to obtain the best duty cycle available.

Counter 4 is a 4-in.-long cylinder of plastic scintillator with a 0.3-in. wall thickness and an inner diameter of 0.20-in. It extends as closely to the counter 3 and to the target as is mechanically possible. It is viewed by a 6810 photomultiplier, and it serves further to collimate the beam, since some particles are multiple-coulomb scattered out of the beam line in counter 3. Another very critical reason for having counter 4 will be discussed below. A metal collimator placed between counter 4 and the target prevents backscattering from the target from cancelling out I_0 events. Counter-4 pulses also pass through a tunnel diode discriminator circuit and are put into anticoincidence. Finally, then, a beam particle is defined by an event of the kind $1\,\overline{2}\,3\,\overline{4}$, and in what follows we understand that the intensity I_0 represents the frequency of events of this kind, i.e. $I_0 = 1\,\overline{2}\,3\,\overline{4}$. In the attuenuation technique utilized here the quantity I_0-I is measured by placing counter 5 (see fig. 1) in anticoincidence, i.e. $I_0 - I = 1\,\overline{2}\,3\,\overline{4}\,\overline{5}$. The advantage of this kind of measurement over measuring I_0 and I separately is obvious.

At the beam levels used in this experiment, significant gain shifts in counter 5 are to be expected. It is therefore extremely difficult to eliminate inelastic events occuring in the target by pulse-height analysis. A simpler and reliable way is to place an energy-degrading foil in front of counter 5 thick enough to stop protons that have been inelastically scattered in the target. The beam energy spectrum will have a tail extending in energy down fron the full energy E by an amount $\delta E = 0.33E$, owing to slit scattering and (p, p') events in the minority isotopes in the lead target. The degrader thickness

could not be great enough so that particles in the tail did not reach counter 5. In practice the degrader was adjusted so that 6.5-MeV protons produced by inelastic events at the center of the target (thickness $\approx$ 1 MeV) were unable to pass through the degrader. The pulse-height distribution in counter 5 was determined to check that the low-energy-tail protons were indeed passing through the degrader, but the data were not usable to further separate inelastic events.

Scattering of beam particles in the target to angles of 60° are detectable with our present arrangement. Scattering through angles of this magnitude can appreciably increase the path length in the target and degrader. This effect is compensated for by decreasing the amount of degrader that the proton must pass through if it is scattered through such an angle (see Fig. 1).

Absorption of the protons occur more frequently in the Al degrader, since it is several times as thick as the targets. This contribution had to be subtracted. This is done by removing the target and placing a "dummy" target in the beam ahead of the scattering foil of such a thickness that the beam energy incident on the degrader foil is the same, and the numbers of i_0 (= 1 $\overline{2}$ 3 $\overline{4}$) and $i_0 - i$ ($\approx$ 1 $\overline{2}$ 3 $\overline{4}$ $\overline{5}$) events are measured.

Since elastic and inelastic scattering cannot in general be neglected, counter 5 must subtend an angle θ large enough so that the elastic scattering $\int_{\theta_5}^{\pi} \sigma_{el}(\theta) d\Omega$ outside the angle θ_5, [where $\sigma_{el}(\theta)$ is the differential elastic-scattering cross section], is not so large that the uncertainty in this quantity limits the accuracy of the measurement. Of course θ_5 is made as small as is possible to reduce the inelastic contribution $\sum_{i=0}^{N} \int_{0}^{\theta_5} \sigma_i(\theta) d\Omega$, where $\sigma_i(\theta)$ is the differential inelastic cross section for the excitation of the ith level of the target element, and the sum extends from the ground state up to the Nth state. Higher-lying states are excluded by the energy resolution afforded by the degrader. By $\sigma_0(\theta)$ we mean the compound elastic differential cross section.

When a "target in" measurement (I_0, I_0-I) and a "dummy in" measurement (i_0, i_0-i) are made, the energy of the proton incident on the degrader is the same in order that absorptive effects in the degrader will be exactly compensated for. However, this has the serious effect of changing the energy that the protons have when they are incident on counter 3 in the two configurations. In the experiment, described here, the energy incident on counter 3 was 10 MeV and 11 MeV in the two configurations, respectively. It turns out that the carbon elastic cross section[19] shows an extraordinarily large resonance in this energy region. Counter 4 in anticoincidence greatly reduces the effect of scattering out. However, the number of protons scattered out at larger angles than the angle θ_4 subtended by counter 4 is still appreciable. The solid line in Fig. 2 shows the value of the quantity

$$\int_{\theta_4}^{\pi} \left[\sigma_{SE}(\theta) + \sum_{i=0}^{1} \sigma_i(\theta)\right] d\Omega = \eta$$

averaged over the energy spread of the protons passing through counter 3, plotted against the energy.[19] The quantity $\sigma_{SE}(\theta)$ is the differential cross section for shape elastic scattering. These data[19] are very comprehensive, so that the correction could be reliably made. As a check, however, the degrader was removed from counter 5, the target was removed, and the quantity $(i_0-i)/i_0$ was measured as a function of beam energy. The beam energy was reduced by the insertion of foils before the lead scattering foil. Squares in Fig. 2 shows the result of this measurement. Anticoincidence events obtained in this configuration are due to reactions or elastic scattering in counter 3. The observation of the position of the resonance in the cross section made a quick and reliable method to measure the beam energy. A quantity $\eta_3 = (\eta_t - \eta_d)$ is defined, where η_t and η_d are the values of η at different energies for two configurations,

i.e., target-in and dummy-in. The scattering-out correction η_3 due to counter-3 events discussed above is obtained from data in Fig. 2 and applied to the measurement. The experimental quantities I_0, I_0-I, i_0, i_0-i, and η_3 are related to the quantity of interest σ_R by the equation

$$\left[\left(\frac{I_0 - I}{I_0\, nx}\right) - \left(\frac{i_0 - i}{i_0\, nx}\right) - \eta_3 \frac{n'x'}{nx}\right] = \sigma_R + \int_{\theta_5}^{\pi} \sigma_{SE}(\theta) d\Omega - \int_0^{\theta_5} \sum_{i=0}^{N} \sigma_i(\theta)\, d\Omega,$$

where n is the target density; x, the target thickness; n', the counter-3 density; and x', the counter-3 thickness. The quantity θ_5 is the angle subtended by counter 5, and $\sigma_{SE}(\theta)$ is the differential shape elastic-scattering cross section $\sigma_{el}(\theta)$-$\sigma_0(\theta)$. Combining the results of this measurement and the elastic scattering data,[5, 19, 20, 21] we obtain the quantity

$$\left[\left(\frac{I_0 - I}{I_0 nx}\right) - \left(\frac{i_0 - i}{i_0 nx}\right) - \eta_3 \frac{n'x'}{nx}\right] - \int_{\theta_5}^{\pi} [\sigma_{SE}(\theta) + \sigma_0(\theta)]\, d\Omega$$

$$= \sigma_R - \int_0^{\pi} \sigma_0(\theta)\, d\Omega - \int_0^{\theta_5} \sum_{i=1}^{N} \sigma_i(\theta)\, d\Omega$$

$$= \sigma_R - \sigma_{CE} - \int_0^{\theta_5} \sum_{i=1}^{N} \sigma_i(\theta)\, d\Omega,$$

where σ_{CE} is the compound elastic cross section, and σ_R is the reaction cross section.

As we improve the energy resolution, the inelastic-scattering term may be reduced but σ_{CE} remains. It may be large compared with the value of σ_R at low energies for light targets. At high energies it generally will be of

negligible importance. For the 10-MeV proton measurements, the compound elastic correction may be very large. Since the inelastic-scattering term can be estimated from inelastic-scattering data,[23] the extracted quantity is $\sigma_R - \sigma_{CE}$, the nonelastic cross section. It should be noted that optical-model calculations generally predict σ_R.

Figure 3 shows a schematic diagram of the electronics. As high gain and good time resolution were needed, the RCA-7264 photomultiplier was chosen for counters 1 and 3. For the other counters, the RCA-6810A photomultiplier was used. At high counting rates ($\approx 10^5$/sec) pulse-height fluctuations may occur in counters 1 and 3 owing to high-current phenomena. This problem was solved by providing voltage to the last five dynodes and the anode directly through cathode followers.

The pulses from counters 1 and 3 were amplified with wide-band amplifiers and put into a Wenzel fast coincidence unit (CC1).[25] Using 10-inch clip lines and large input pulses (3 volts) made it possible to obtain 2 mμsec resolving time. For anticoincidences the unit was found to work best with large constant-size pulses (6 volts). To accomplish this, a tunnel diode discriminator[18] producing a constant output pulse was used on all pulses for anticoincidence. The tunnel diode discriminator unit differentiates the incoming pulse and fires on the zero crossover point. this eliminates, to a large extent, the characteristic time jitter of the usual fast discriminators and preserves good time resolution. Three coincidence units called CC1, CC2, and CC3 (see Fig. 3) were needed to accommodate the anti-pulses. The output of CC1 was fed into CC2 and the CC2 output fed into CC3. Counter 3 was carried through all units in order to eliminate the possibility that noise would trigger the circuit. A slower resolving time was used in CC2 and CC3 because the fast resolving time from CC1 is automatically carried through these units. Scaling the output of CC2 gives $1\ \overline{2}\ 3\ \overline{4}$ or I_0, and CC3 gives $1\ \overline{2}\ 3\ \overline{4}\ \overline{5}$ or $I_0 - I$. The output of CC3 was used also as the gate pulse for a fast linear gate unit.[26] A fast linear pulse from counter 5 with appropriate

delay is fed into the linear gate. If the gate is open this signal is further amplified and stretched and fed into a 400-channel pulse-height analyzer. The capacitance feed-through on the linear gate is adjusted so that a small pulse is sent to the pulse-height analyzer even though no linear signal from counter 5 was coincident with it. The resulting peak in the pulse-analyzer spectrum is named the "miss peak."

The counter-5 tunnel diode discrimator is adjusted so that any pulse height below the full-energy peak height will give rise to a CC3 output pulse. A sample spectrum is shown in Fig. 4. The miss peak contains the (p, n) events and those (p, p') events in which the inelastic proton fails to traverse the degrader, i.e., all inelastic events in which the outgoing proton energy $Ep' \leq 6.5$ MeV. In Fig. 4, events in channels 15 to 24 are inelastic events ($6.5 \text{ MeV} \leq Ep' \leq 7.4 \text{ MeV}$). The events above channel 24 include inelastic events with outgoing proton energy ≥ 7.4 MeV and the low-energy tail of the incident beam. In this energy region no separation can be made between these two, since the time-of-flight separation system is capable of separating out only protons with energy ≤ 7.4 MeV (see discussion of time-of-flight method at the beginning of this section). The cutoff at about channel 64 (9.5 MeV) is at the lower side of the full energy peak.

For setting up the electronics, an experimental procedure was followed that minimized the check-out time and gave the most consistent results. First, the pulse heights and delays from the counters into the three coincidence units were all checked and set at optimum values. The thresholds on the three-tunnel diode discriminator from counters 2, 4, and 5 were then set as low as possible. Antidiscriminator curves were then taken. The number of counts in the miss peak for a fixed I_0 value was plotted against the CC1, CC2, and CC3 10-Mc discriminator settings to obtain discriminator curves. Experimental parameters were carefully adjusted in order to obtain flat anticoincidence

discriminator plateaus. With the CC discriminators set at the values obtained, the number of counts in the miss peak for a fixed I_0 value was measured as a function of counter-1 delay time (see Fig. 5). The minimum occurs at a relative delay of approximately 1.8 mμsec. If the delay is decreased, a rise in the number of counts in the miss peak for $I_0 = 2\times10^6$ is observed. This effect is contributed to by two kinds of events. First, by protons of energy ≤ 6.5 MeV yield large delay-line-clipped pulse heights into the coincidence circuit. Consequently they may fire the I_0 circuit and cause a count in the miss peak even though the delay setting is unfavorable. Secondly, elastic, inelastic, and (p, q) events (where q is a charged particle) that occur in counter 3 may contribute. Such an event is counted most efficiently at short delays and of course contributes to the miss peak. This is due to the early firing of the coincidence circuit by the large pulse from counter 3 when an event of this type occurs. The sharp rise in the number of counts in the miss peak for longer delays (see Fig. 5) is due to the fact that protons in the low-energy tail are counted most efficiently at longer delays. Low-energy protons contribute relatively more counts in the miss peak. The minimum in this curve, then, is the point at which the coincidence time-of-flight technique is working at its best.

III. REACTION CROSS SECTION RESULTS

The raw data for the measurements on Be, Cu, Ag, and Au targets are listed in Table I. Target thicknesses are adjusted to be 1 MeV thick. In order for the contribution of the error due to counting statistics to be comparable to or smaller than contributions due to other sources of error, it was necessary that $I_0 \approx 2\times10^7$. For the Be target, the resulting statistical uncertainty in the reaction cross-section measurement is about 1%, whereas for the Ag and Cu targets the statistical uncertainty in this quantity is about 3% owing essentially to the smaller number of target atoms per square centimeter in

these targets.

The counter 3 correction η_3 n'x'/nx varies in importance. For a Be target it is a 0.2% correction at 10.12 MeV and a correction 3.5% at 9.90 MeV; whereas for Ag, it is 0.7% at 10.12 MeV and 10% at 9.90. Fortunately it may be obtained accurately by the method outlined above. The values of σ, the raw cross section, are listed in the last column of Table I. They must be corrected for elastic and inelastic scattering. These corrections are listed in Tables II (a) and II (b).

Tables II(a) and II (b) are a summary of data obtained. The raw cross sections, σ (some of which are listed in the last column of Table I), are listed in the second column. In the third column the elastic corrections are listed, and reference numbers to the data used to make the corrections are given. Wherever experimental data on elastic scattering were available, they were integrated between the proper limits and listed in the table. In some instances elastic-scattering data were available at nearby energies. Interpolation or extrapolation of this data was sometimes possible. Optical-model calculations were kindly made available to us be Dr. E. Schwarcz in order to check those cases in which the extrapolation or interpolation was severe. Dr. Schwarcz has used the results of the Fernbach-Bjorklund optical-model analysis[15] to obtain these results. The same situation obtains for the inelastic scattering data at the angles subtended by counter 5. However, the correction[23,24] was a great deal smaller than the elastic-scattering correction [see Tables II (a) and II (b)].

It is to be noted that for Au, Th, Pb, and Ta the elastic-scattering correction is very large. Therefore, although we measure σ with a statistical accuracy of about 2 %, we know $\sigma_R - \sigma_{CE}$ only to about ± 40% for these heavy elements. Thus it is difficult to measure $\sigma_R - \sigma_{CE}$ for heavy elements with good accuracy at 10 MeV. We may use σ for heavy elements, however, as a

check on the reliability of our results, since elastic-scattering data exist for Au in particular, and show that elastic-scattering correction is nearly equal to the correction that would obtain for coulomb scattering from a point charge. Thus the sum of the elastic correction and the optical-model value for σ_R From the work of Fernbach and Bjorklund[15] should be quite close to the correct value for this quantity, since deviations in σ_R from the optical-model value will cause small errors in the sum of these two quantities. Our measured values of σ for Au agree, within the statistical uncertainty of 2%, with the theoretical value.

In Fig. 6 the predicted reaction cross sections σ_R at 10 MeV for a surface absorption potential[15] that fit the elastic-scattering data are plotted. Also plotted are the measured values of $\sigma_R - \sigma_{CE}$. The agreement with the results from the surface-absorption model is qualitatively good for $A^{2/3} > 16$, although the measured values tend to be systematically larger. The solid and dashed curves representing the optical-model predictions show the change in the cross section resulting from the beam energy difference on the two experimental runs when the data were collected. The experimental points systematically reflect a similar difference. For $A^{2/3} < 16$, the strong minima near Ni and C cause large deviations from the predictions, but it should be emphasized that we measure $\sigma_R - \sigma_{CE}$. It is quite possible that these deep minima may be due to resonances in σ_{CE} near C and Ni. Such an interpretation of neutron reaction cross-section data has been suggested by Perey.[28] At 10 MeV, C is certainly expected to have a large cross section for σ_{CE}. Because of the high (p, n) threshold, 18 MeV, only two states, the ground state and the first excited state, are appreciably populated from the compound nucleus at 10 MeV.[29] One expects these states to be roughly of equal intensity, thus explaining the deep minimum we get in $\sigma_R - \sigma_{CE}$ for C.

An alternative viewpoint, that the minimum in the vicinity of Ni is associated with σ_R, cannot be ruled out. This would imply that the nuclear area presented to the projectile shrinks by about 12% in the vicinity of the proton closure at 28 protons, or a size resonance occurs.[10] Measurements of 40-MeV alpha-particle reaction cross sections (soon to be reported) also show a minimum near Z = 28. This tends to support the viewpoint that the nucleus shrinks there, since σ_{CE} should be insignificant at 40 MeV for alpha particles and size resonances should have a small effect.

Figure 7 shows the predicted range of values for the reaction cross section by use of a Woods-Saxon potential (volume absorption) adjusted to fit the elastic-scattering data. The experimental reaction cross section is not inconsistent with the upper limit predicted by volume absorption. Note in Fig. 7 that the calculations were for specific elements.[3, 30] As an example, the range of reaction cross sections predicted as in Fig. 7 in the vicinity of $A^{2/3} = 16$ should be compared with the Cu data point and not with the experimental measurements for nearby elements. For larger values of $A^{2/3}$ the shaded bar represents only regions where good fits could be obtained and does not necessarily represent limits of σ_R. Although greatly restricting the sets of parameters that one may use, the σ_R data have not yet enabled one to choose between surface and volume absorption.

Figure 8 is a plot showing all the experimental data available near 10 MeV plotted as a function of $A^{2/3}$. The agreement between the trend of the data of Albert and Hansen,[9] of Wing and Huizenga,[10] and our data is satisfactory. The reaction cross section measurements for Cu at about 9 MeV are also plotted.[8, 12] These have been measured by the attenuation technique. These values are larger than our results and the results from the summation technique. Since they are measured at 9 MeV, they would be expected to be smaller to be in accord, because of the effects of the coulomb barrier.

It has been pointed out earlier that reaction cross sections near the barrier height should be particularly sensitive to the shape of the optical-model potential. It is in the vicinity of $A^{2/3}=24$ that the cross sections reach a maximum and therefore the sensitivity to changes in optical parameters is maximized in this region. There appears to be a systematic deviation between current optical-model calculations and our measured reaction cross sections in this region.

Table I. The experimental quantities obtained in the measurement of $\sigma_R - \sigma_{CE}$. The column heads are defined in the text, except σ, which is $\frac{I_0 - I}{I_0\, nx} - \frac{i_0 - i}{i_0\, nx} - \eta_3 \frac{n'x'}{n\,x}$.

Beam energy MeV	Element	Target thickness (mg/cm^2)	I_0 ($\times 10^6$)	$I_0 - I$	i_0 ($\times 10^6$)	$i_0 - i$*	$I_0 \eta_3 n'x'$	$n\,x\,\sigma$ ($\times 10^{-3}$)	σ (mb)
10.15	Be	23.57	20.115	34007	20.000	14466	+45	1.0171	672
9.93	Be	23.57	20.000	31921	20.000	12152	-754	0.9507	605
10.12	Cu	36.70	20.011	21181	20.000	14466	+40	0.3334	1000
9.90	Cu	36.70	20.000	19446	20.000	12164	-764	0.3259	940
10.12	Ag	43.05	20.516	21239	20.000	14466	+40	0.3125	1312
9.90	Ag	43.05	20.000	18978	20.000	12162	-762	0.3027	1258
10.12	Au	54.46	20.015	24841	20.000	14466	+40	0.5101	3068
9.90	Au	54.46	20.000	22840	20.000	12162	-762	0.4958	2952

*Average of four runs.

Table II (a). The raw cross section σ, the elastic-scattering correction, inelastic-scattering correction $\sigma_R - \sigma_{CE}$, and the lab energy at the center of the target. A lead scattering foil enriched to 94% Pb^{208} is used in these measurements.

Energy	σ	$\int_{\theta_5 = 60.2^\circ\ (lab)}^{\pi} [\sigma_{SE}(\theta) + \sigma_0(\theta)]\, d\Omega$	$\int_0^{\theta_5 = 60.2^\circ\ (lab)} \sum_{i=1}^{N} \sigma_1(\theta) d\Omega$	$\sigma_R - \sigma_{CE}$
(MeV)	(mb)	(mb)	(mb)	(mb)
Be 10.15± .47	672± 10	89± 5[5]	80± 8[24]	663± 14
C 10.16± .46	618± 13	286± 14[19]	0*	332± 19
Al 10.12± .50	797± 24	190± 10[5]	97± 10[23]	704± 28
Au 10.12± .50	3068± 59	2895± 89[5]	0*	173± 107
Cu 10.12± .50	1000± 41	215± 11[5]	31± 3[23]	816± 43
Zn 10.12± .50	994± 41	193± 10[20, 22]	49± 5[23]	850± 43
Ag 10.12± .50	1312± 57	630± 32[5]	7± 1[23]	689± 65
Ni 10.14± .48	834± 40	223± 11[5]	89± 9[23]	700± 42
Rh 10.14± .48	1303± 57	562± 42[27]	10± 5*	751± 71
Nb 10.17± .45	1172± 57	483± 37[22]	15± 5*	703± 68
Ti 10.22± .40	902± 43	116± 9[20]	44± 4[23]	830± 44
Fe 10.20± .42	853± 45	148± 11[20, 27]	54± 5[23]	759± 47
Ta 10.20± .42	2508± 119	2179±164[27]	2± 1*	331± 203
Sn 10.21± .41	1522± 72	803± 40[5]	4± 1[23]	723± 82
Zr 10.25± .37	1233± 72	453± 45*	20± 5*	800± 85

*Estimates from interpolation of other data.

Table II (b). The raw cross section σ, the elastic-scattering correction $\sigma_R - \sigma_{CE}$, and the lab energy at the center of the target. A thorium scattering foil was used in these measurements.

Energy (MeV)	σ (mb)	$\int_{\theta_5 = 62.1^\circ\,(\text{lab})}^{\pi} [\sigma_{SE}(\theta) + \sigma_0(\theta)]d\Omega$ (mb)	$\int_0^{\theta_5 = 62.1^\circ\,(\text{lab})} \sum_{i=1}^{N} \sigma_1(\theta)d\Omega$ (mb)	$\sigma_R - \sigma_{CE}$ (mb)
Be 9.93± .47	605± 10	92± 5[5]	80± 8[23, 24]	593± 14
C 9.94± .46	504± 13	275± 14[19]	0[29]	229± 19
Al 9.90± .50	744± 24	185± 10[5]	97± 10[23]	656± 28
Au 9.90± .50	2952± 58	2790± 86[5]	0*	162± 104
Cu 9.90± .50	940± 41	216± 11[5]	31± 3[23]	755± 43
Zn 9.90± .50	883± 41	203± 10[20, 22]	49± 5[23]	729± 43
Ag 9.90± .50	1258± 57	603± 30[5]	7± 1[23]	622± 64
Ni 9.92± .48	766± 40	220± 11[5]	89± 9[23]	635± 42
Nb 9.95± .45	1161± 57	453± 36[22]	15± 5*	723± 68
Ti 9.99± .41	887± 43	114± 9[20]	44± 4[23]	817± 44
Fe 9.97± .43	820± 45	146± 11[20, 27]	54± 5[23]	728± 47
Ta 9.98± .42	2496± 119	2110± 160[27]	2± 1*	388± 195
Sn 9.99± .41	1374± 72	768± 38[5]	4± 1[23]	610± 82
Zr 10.03± .37	1197± 72	424± 42*	20± 5*	793± 83
Mo 10.03± .37	1168± 72	467± 47*	20± 5*	721± 86
Th 9.98± .42	3550± 108	3615± 108*	0*	-65± 153
Pb 9.92± .48	3266± 100	3050± 110*	0*	216± 148
V 9.96± .44	1082± 40	320± 48*†	20± 3[23]†	782± 62

* Estimates from interpolation of other data.
† $\theta_5 = 48.6^\circ$.

ACKNOWLEDGMENTS

The authors are indebted to W. B. Jones and the rest of the crew at the 60-inch cyclotron for providing us with a steady proton beam. We wish to thank E. Schwarcz for the use of his optical-model calculations. Our thanks are also due to N. M. Hintz, who made available to us his (p, p') data at 10 MeV.

REFERENCES

1. T. Gooding, Nucl. Phys. 12, 241 (1959).
2. V. Meyer, R. M. Eisberg, and R. F. Carlson, Phys. Rev. 117, 1334 (1960).
3. A. E. Glassgold, W. B. Cheston, M. L. Stein, S. B. Schuldt, and G. W. Erickson, Phys. Rev. 106, 1207 (1957).
4. R. D. Woods and D. S. Saxon, Phys. Rev. 95, 577 (1954).
5. N. M. Hintz, Phys. Rev. 106, 1201 (1957).
6. G. W. Greenlees, (University Institute for Theoretical Physics, Copenhagen, Denmark), private communication.
7. V. Meyer and N. M. Hintz, Phys. Rev. Letters 5, 207 (1960).
8. G. W. Greenlees and O. N. Jarvis, in Proceedings of International Conference on Nuclear Structure (University of Toronto Press, Toronto, Canada, (1960) p. 217.
9. R. D. Albert and L. F. Hansen, Phys. Rev. 123, 1749 (1961).
10. J. Wing and J. R. Huizenga, (p, n) Cross Sections of V^{51}, Cr^{52}, Cu^{43}, Cu^{65}, Ag^{107}, Ag^{109}, Cd^{111}, Cd^{114}, La^{139} from 5 to 10.5 MeV, submitted to Phys. Rev.
11. J. Benveniste, R. Booth, and A. Mitchell, Phys. Rev. 123, 1818 (1961).
12. R. F. Carlson, R. M. Eisberg, R. H. Stokes, and T. H. Shirt, University of Minnesota Annual Progress Report, 1961.
13. R. E. Pollock and G. Schrank, Bull. Am. Phys. Soc. 7, 72 (1962).
14. J. M. Blatt and V. F. Weisskopf, Theoretical Nuclear Physics (J. Wiley and Sons, New York, 1952), p. 379.
15. F. Bjorklund and S. Fernbach, Phys. Rev. 109, 1295 (1958).

16. B. Easlea and G. E. Brown, in Proceedings of International Conference on Nuclear Structure(University of Toronto Press, Toronto, Canada, 1960), p. 219.

17. P. E. Hodgson, in Proceedings of Rutherford Jubilee International Conference (Heywood and Company Ltd., London, 1961), p. 357.

18. A. E. Bjerke, Q. A. Kerns, and T. A. Nunamaker, Lawrence Radiation Laboratory Report UCRL-9838, 1961.

19. Y. Nagahara, J. Phys. Soc. Japan 16, 133 (1961).

20. K. Kikuchi, S. Kobayashi, and K. Matsuda, J. Phys. Soc. Japan 14, 121 (1959).

21. C. Hu, K. Kikuchi, S. Kobayashi, K. Matsuda, Y. Nagahara, Y. Oda, N. Takano, M. Takeda, and T. Yamazaki, J. Phys. Soc. Japan 14, 861 (1959).

22. G. W. Greenlees, L. Gioietta Kuo, M. Petravic, Proc. Roy. Soc. (London) A 243, 206 (1958).

23. N. M. Hintz, (University of Minnesota), private communication.

24. R. G. Summers-Gill, Phys. Rev. 109, 1591 (1958).

25. W. A. Wenzel, Lawrence Radiation Laboratory Report UCRL-8000, (1957).

26. G. B. B. Chaplin and A. J. Cole, Nucl. Instr& Methods 7, 45 (1960).

27. E. Schwarcz, (Lawrence Radiation Laboratory), private communication.

28. F. G. J. Perey, (Oak Ridge National Laboratory), private communication.

29. H. E. Conzett, Phys. Rev. 105, 1324 (1957).

30. J. S. Nodvik and D. S. Saxon, Phys. Rev. 117, 1539 (1960).

Figure Captions

Fig. 1. Schematic diagram of the experimental area.

Fig. 2. Beam energy calibration curve. The solid curve and the symbol ● represent the Japanese elastic scattering data[19] suitably integrated over the energy loss in counter 3. The symbol ▣ represents the experimental points from this work.

Fig. 3. Schematic diagram of the electronics.

Fig. 4. Counter 5 pulse-height spectrum.

Fig. 5. The miss peak vs. the variable delay on counter 1. The arrow indicates the position chosen for the runs.

Fig. 6. Proton $\sigma_R - \sigma_{CE}$ around 10 MeV: ● - the experimental points at 10.1 to 10.2 MeV, ▣ - the experimental points at 9.9 to 10.0 MeV. The solid and dashed curves are the theoretical predictions of σ_R at 10.1 and 9.9 MeV, using an optical model with surface absorption.[9, 15]

Fig. 7. Proton reaction cross sections showing predictions using both volume and surface absorption. The symbol ● represents the experimental points; the solid curve, surface absorption predictions of Bjorklund and Fernbach; and ▨, range of values predicted by the Woods-Saxon potential (volume absorption) as calculated by Glassgold et al.[3] and Nodvik and Saxon.[30]

Fig. 8. All experimental data in the region of 10 MeV plotted as function of $A^{2/3}$:

Results of this experiment;

from Albert and Hansen (p, n)[9] and Meyer and Hintz (p, q);[7]

from Wing and Huizenga (p, n)[10] and Meyer and Hintz (p, q);[7]

from Greenlees and Jarvis;[8] from Carlson et al;[12] and from Nagahara.

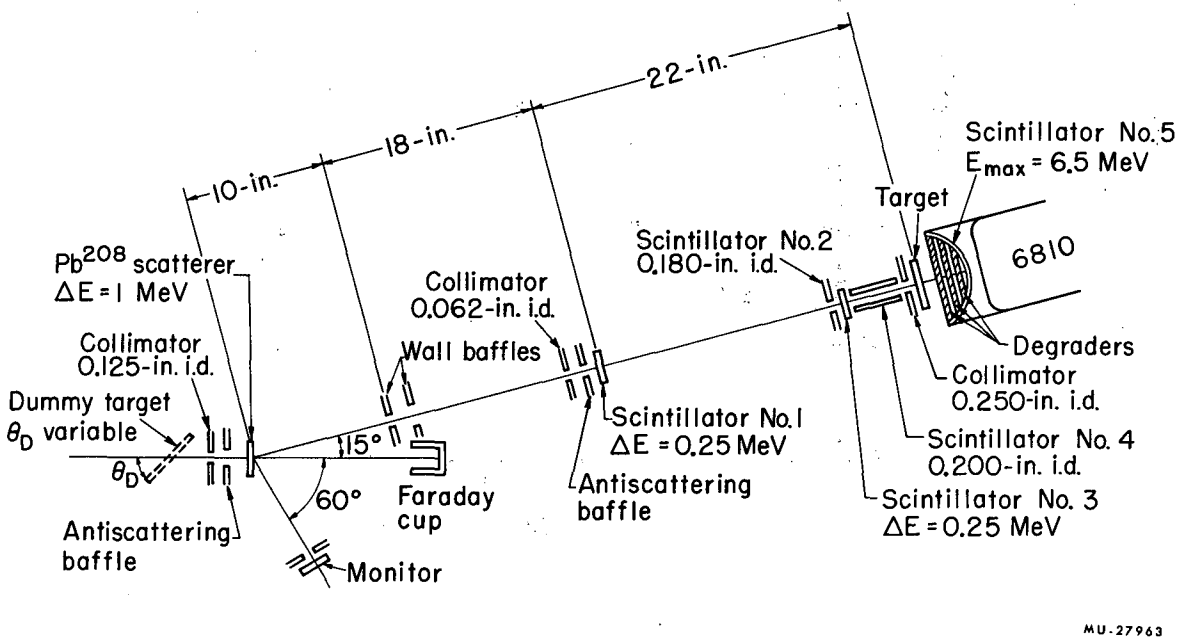
22-in.
18-in.
10-in.
Scintillator No.5
E_{max} = 6.5 MeV
Target
6810
Scintillator No.2
0.180-in. i.d.
Pb^{208} scatterer
ΔE = 1 MeV
Collimator
0.062-in. i.d.
Wall baffles
Collimator
0.125-in. i.d.
Dummy target
θ_D variable
θ_D
15°
60°
Faraday
cup
Monitor
Antiscattering
baffle
Scintillator No.1
ΔE = 0.25 MeV
Antiscattering
baffle
Degraders
Collimator
0.250-in. i.d.
Scintillator No. 4
0.200-in. i.d.
Scintillator No. 3
ΔE = 0.25 MeV
MU-27963

Fig. 1

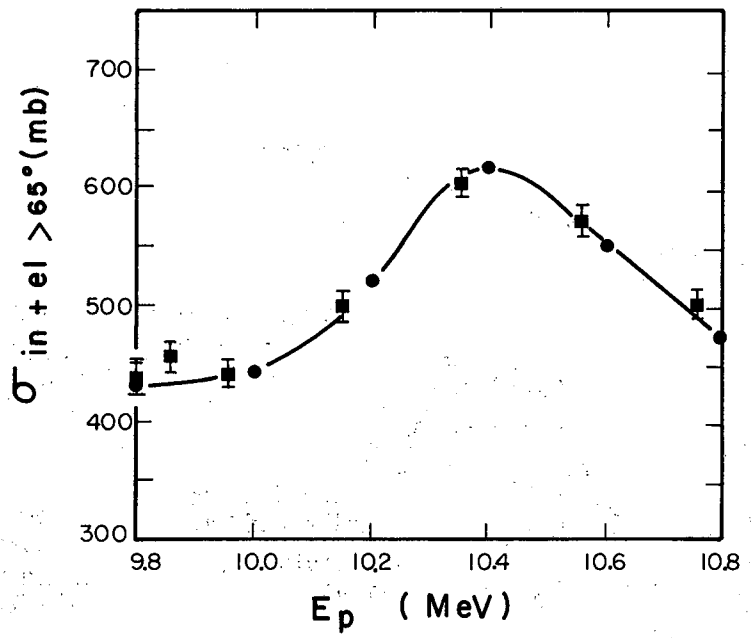
700
600
500
400
300
σ in + el >65°(mb)
9.8
10.0
10.2
10.4
10.6
10.8
Ep (MeV)
MU-27141

Fig. 2

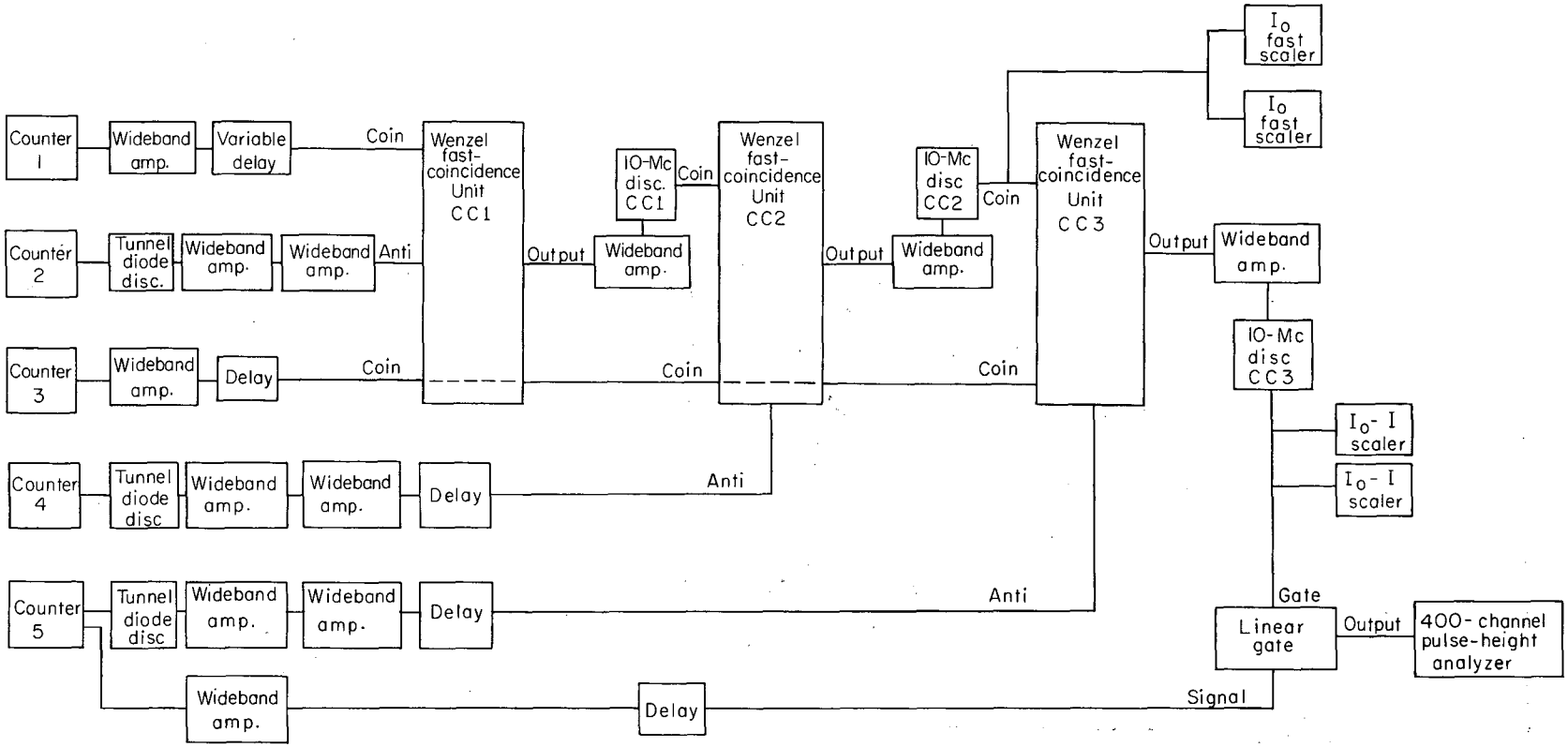

Fig. 3

UCRL-10281

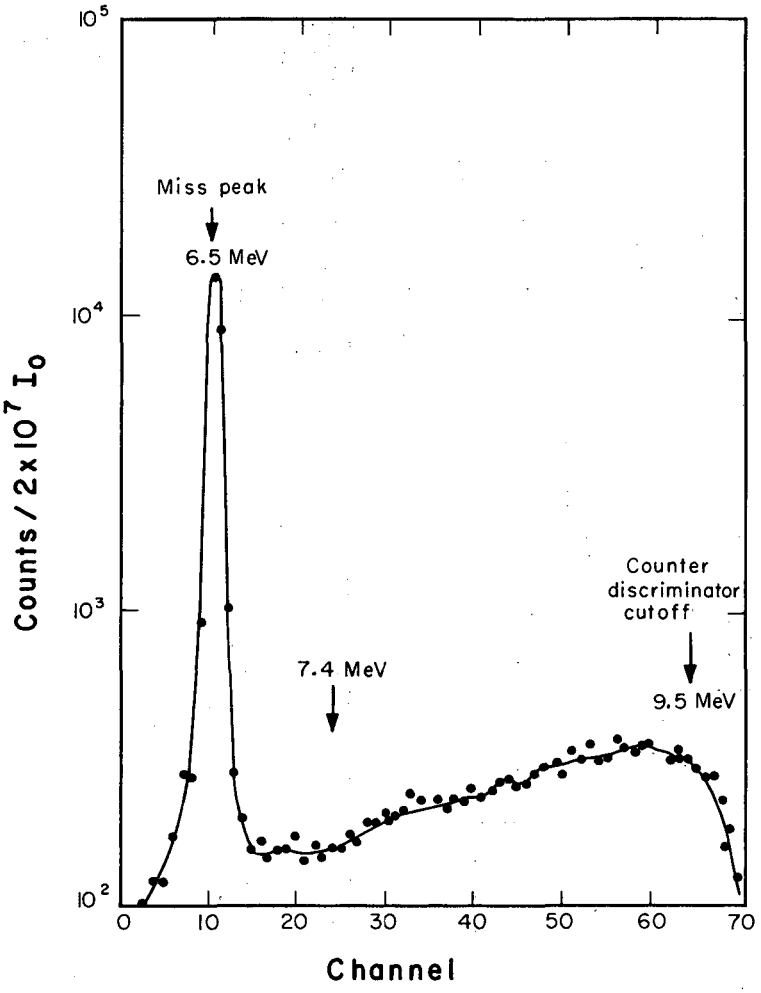
Miss peak
6.5 MeV
7.4 MeV
Counter discriminator cutoff
9.5 MeV
Counts / 2x10^7 I_0
Channel
MU-27139

Fig. 4

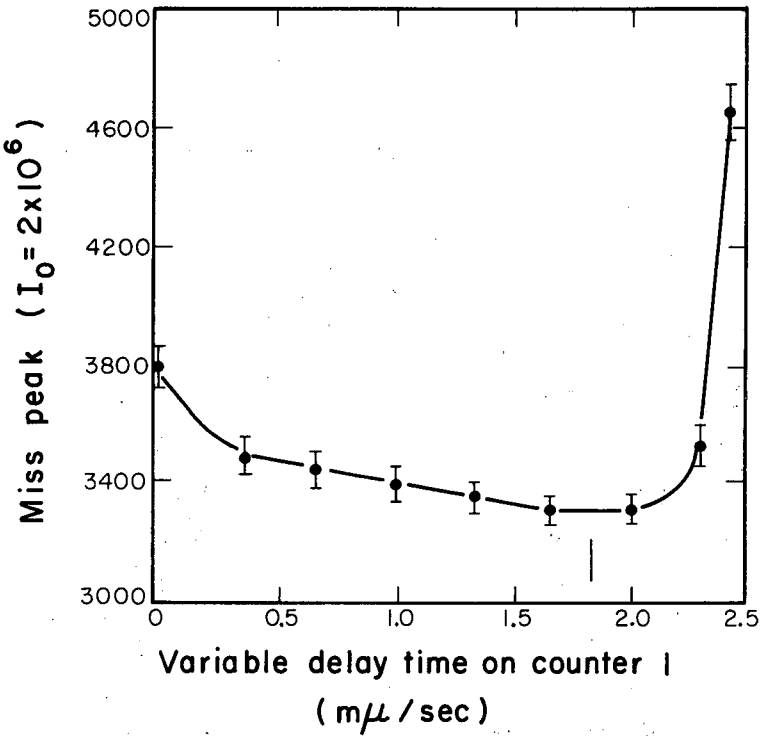
5000
4600
4200
3800
3400
3000
Miss peak (I_0= 2x10^6)
0
0.5
1.0
1.5
2.0
2.5
Variable delay time on counter I
(mμ/sec)
MU-27138

Fig. 5

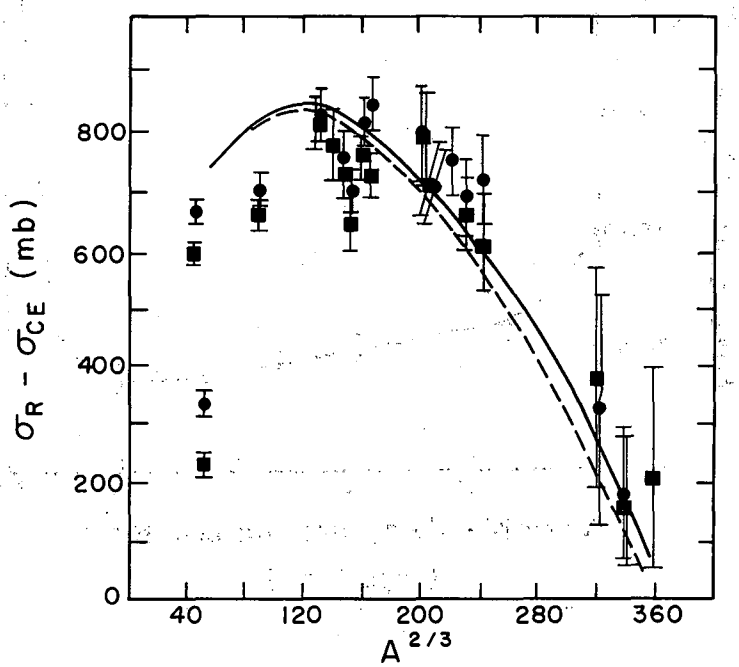
$\sigma_R - \sigma_{CE}$ (mb)
800
600
400
200
0
40
120
200
280
360
$A^{2/3}$
MU-27135

Fig. 6

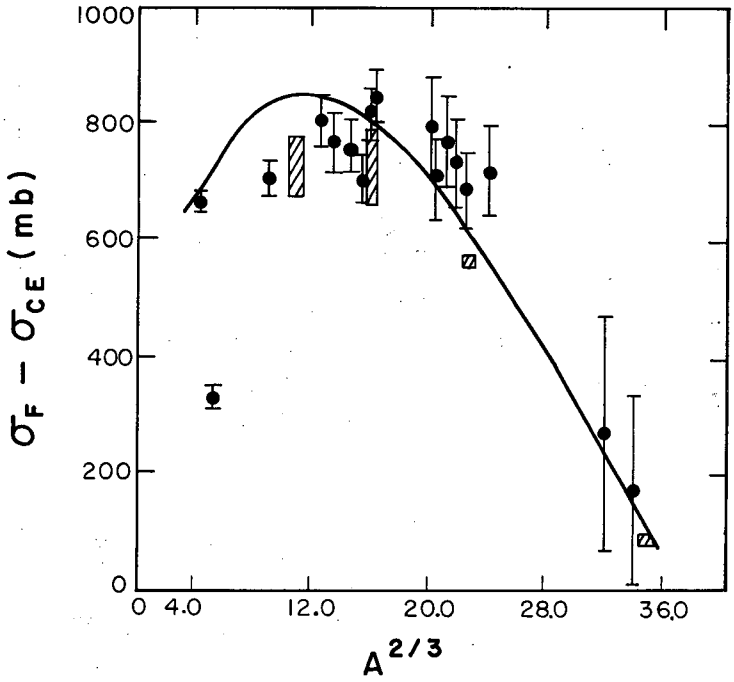
1000
800
600
400
200
0
0 4.0
12.0
20.0
28.0
36.0
$\sigma_F - \sigma_{cE}$ (mb)
$A^{2/3}$
MU-27140

Fig. 7

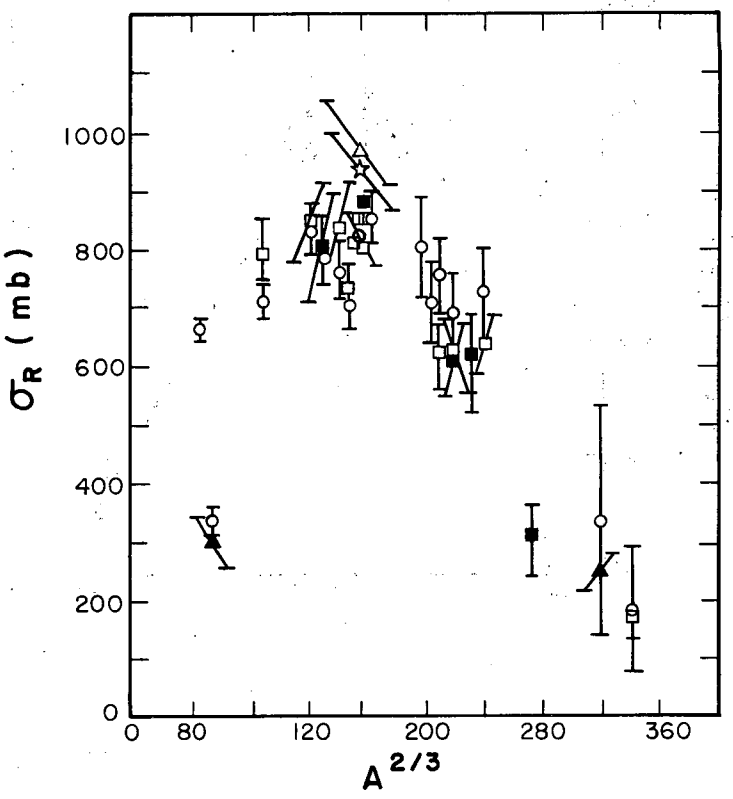
1000
800
600
400
200
0
σ_R (mb)
0
80
120
200
280
360
$A^{2/3}$
MU-27137

Fig. 8